

# Ultracold neutron accumulation in a superfluid-helium converter with magnetic multipole reflector

O. Zimmer<sup>1</sup> and R. Golub<sup>2</sup>

<sup>1</sup>Institut Laue Langevin, 38042 Grenoble, France

<sup>2</sup>Department of Physics, North Carolina State University, Raleigh, NC 27695, USA

June 4, 2018

## Abstract

We analyze accumulation of ultracold neutrons (UCN) in a superfluid-helium converter vessel surrounded by a magnetic multipole reflector. We solved the spin-dependent rate equation, employing formulas valid for adiabatic spin transport of trapped UCN in mechanical equilibrium. Results for saturation UCN densities are obtained in dependence of order and strength of the multipolar field. The addition of magnetic storage to neutron optical potentials can increase the density and energy of the low field seeking UCN produced and serves to mitigate the effects of wall losses on the source performance. It also can provide a highly polarized sample of UCN without need to polarize the neutron beam incident on the converter. This work was performed in preparation of the UCN source project SuperSUN at the ILL.

Keywords: ultracold neutrons, UCN source, neutron EDM, neutron decay

## 1 Introduction

Mirror reflection of neutrons is an effect of the neutron optical potential which is mainly due to coherent s-wave scattering of neutrons by atomic nuclei in condensed matter [1]. Ultracold neutrons (UCN), which were first produced in Dubna [2] and in Munich [3], have energy sufficiently low to become totally reflected under any angle of incidence. This peculiar property enables experimentalists to store them in "neutron bottles" made of suitable materials with small cross sections for neutron absorption and providing well depths up to about 300 neV [4, 5]. Storage time constants of many hundreds of seconds and the possibility to employ also magnetic fields and gravity for trapping and manipulation have made UCN a versatile tool to investigate various phenomena of fundamental physics complementary to experiments at high-energy particle accelerators [6, 7, 8].

Among recent experiments with UCN feature a first demonstration of gravity resonance spectroscopy with the goal to search for deviations from Newton's gravity law at the micrometer length scale [9], searches for "mirror dark matter" [10, 11], a test of Lorentz invariance [12], searches for axion-like particles [13, 14, 15], a demonstration of the effect of accelerated matter on the neutron wave [16] and of the stability of the Berry geometrical phase for spin  $\frac{1}{2}$  particles under the influence of noise fluctuations [17]. Earlier work with UCN on the geometrical phase was published in [18, 19], while its first demonstration with cold neutrons can be found in [20].

Long standing are efforts to improve the accuracy of the weak axial-vector and vector coupling constants of the nucleon derived from precise values of the neutron lifetime [21, 22, 23, 24, 25] and the beta-asymmetry [26, 27, 28, 29]. Among other applications these values are crucial

input for calculations of weak reaction rates in big-bang nucleo-synthesis and stellar fusion [30, 31], and of the efficiency of neutrino detectors [32]. Also long standing is the search for a non-vanishing neutron electric dipole moment (EDM), which would violate the symmetries of parity (P) and time reversal (T) and thus via the CPT theorem also the combined symmetries of charge conjugation and parity (CP). This search was proposed already in 1950 by Purcell and Ramsey [33] and has become a prominent route to investigate new mechanisms of CP violation beyond the standard model's complex phase of the weak quark mixing CKM matrix, and the matter-antimatter asymmetry in the universe [34]. At the present best level of sensitivity, still no EDM was observed [35]. Several projects are in preparation or underway with the goal to gain at least an order of magnitude in sensitivity [36, 37, 38, 39, 40, 41, 42, 43, 44].

Most studies with UCN are counting statistics limited and will strongly profit from new UCN sources which are currently being developed in various laboratories around the world [45, 46, 47, 48, 49, 50, 51, 52, 53, 54]. They are all based on the "superthermal" UCN production scheme proposed in 1975 by one of the authors together with Mike Pendlebury [55], using either superfluid  $^4\text{He}$  or solid deuterium as a medium for neutron conversion. Early milestones in the development of the latter were published in [56, 57, 58]. Here we focus on UCN production in a converter of superfluid  $^4\text{He}$  installed at the end of a neutron guide, wherein neutrons with energy 1 meV, respectively, wavelength 0.89 nm may lose nearly their entire energy in single scattering events. At low temperature only few excitations are present in the helium that are able to scatter UCN back to higher energies. With the vanishing absorption cross section of  $^4\text{He}$  it becomes possible to accumulate UCN within a converter with reflective boundaries before releasing them to an experiment at room temperature. While an earlier attempt to bring this technique to life was hampered by extraction losses (nonetheless producing record UCN densities for its time) [59], a more efficient method was developed recently by one of the authors together with his co-workers [47, 60, 61, 62]. UCN are extracted through a cold UCN valve and a short vertical UCN guide section, superseding lossy separation window, screens and gaps for thermal insulation between the converter and the UCN guide of the earlier scheme. Work is in progress to bring the technique to maturity for a new user facility at the ILL, and in particular for performing a neutron lifetime experiment using magnetic trapping [63, 64, 65]. Also other groups have recognized the potential advantages of a superfluid helium converter feeding UCN to experiments at room temperature [50, 51], and in some experiments this type of converter is employed in situ [39, 43, 66].

The efficiency of a UCN accumulator at an external neutron beam relies on loss rates being sufficiently low. Most critical are those losses which occur when UCN hit the walls of the converter vessel. They are proportional to the frequency of collisions and thus depend on the size and shape of the converter vessel. From transmission measurements through superfluid  $^4\text{He}$  at 1.25 K a mean free path of 17 m was derived for the 0.89 nm neutrons most effective for UCN production [67]. Hence, the vessel can be made several meters long without significant reduction in UCN density. On the other hand, the lateral dimensions of the converter vessel should match the size of the available neutron beam and guide it to avoid dilution of the incident flux. The mean free path of UCN in a vessel with such geometry is therefore only in the order of 5 – 10 cm, leading to high typical frequencies of UCN wall collisions of 50 – 100 per second. It thus becomes challenging to obtain long UCN storage time constants which however are a prerequisite for accumulation of a high saturated UCN density. Values measured for narrow vessels are normally well below 200 s. For instance, in a recent experiment on UCN production, a rather short storage time constant of 67 s was obtained for a vessel held at 0.7 K, which consisted of a 1 m long  $7 \times 7 \text{ cm}^2$  tube of BeO with Be windows on each end and included a short pipe from stainless steel. That, nonetheless, a record UCN density was obtained demonstrates the potential of the method [60]. To our knowledge the Cryo-EDM collaboration achieved with  $\tau = 160 \text{ s}$  the so far highest value for a helium converter enclosed within matter boundaries,

using a 3 m long tubular vessel with diameter 63 mm, made of Be coated copper and closed off by Be windows [39].

Magnetic trapping of UCN offers a viable way for a drastic improvement of the storage properties of the converter vessel, ultimately limited only by the neutron lifetime  $\tau_\beta \approx 880$  seconds. It relies on the potential energy  $\pm\mu_n B$  of the neutron magnetic moment  $\mu_n \approx 60$  neV/T in a magnetic field  $B$ . Suitable configurations of magnetic field gradients keep the low field seeking UCN away from walls where otherwise the collisional losses occur. A group at NIST has demonstrated storage time constants consistent with the neutron lifetime within a helium converter equipped with a superconducting magnetic quadrupole UCN reflector [68, 66]. The apparatus was designed to perform neutron lifetime measurements, for which a complete suppression of UCN wall contacts is mandatory. On the other hand, for the sake of enhancing the output of a UCN source, combined magnetic and material trapping turns out to be particularly beneficial. In addition, the phase space for UCN accumulation can be much increased using a higher multipole order.

In this paper we provide an analytic treatment of the rate equation for UCN production and storage in a superfluid-helium converter confined by material walls and surrounded by a magnetic mirror. We show that, combining a converter vessel possessing good (but not exceptional) storage properties with a magnetic mirror of high multipole order, one may achieve a saturated UCN density close to the theoretical limit defined by an ideal experimental bottle, i.e. a square well potential without imaginary part. That the magnet needs to generate only part of the trapping potential is of great practical value for constructing a device using standard superconducting wire technology.

## 2 Rate equation and system definition

The temporal evolution of the spectral UCN density in a closed converter irradiated with the cold beam is governed by a simple rate equation. UCN production is characterized by a spectral rate density  $p$  that depends on the spectral flux of the incident beam, and a loss term is due to finite lifetime  $\tau$  of UCN in the converter,

$$\frac{dn(\epsilon_0, t)}{dt} = p(\epsilon_0) - \frac{n(\epsilon_0, t)}{\tau(\epsilon_0)}. \quad (1)$$

Here we label stored neutrons by their total energy  $\epsilon_0$ , defined as their kinetic energy at the point of lowest potential energy in the trap. The quantities  $n(\epsilon_0, t)$  and  $p(\epsilon_0)$  denote the real space density, respectively, the spatial UCN production rate density, each per energy interval of a group of UCN with total energy in the range  $(\epsilon_0, \epsilon_0 + d\epsilon_0)$ . The saturated spectral UCN density obtains when UCN losses balance UCN production for  $t \gg \tau$  after having switched on the beam. It is given by

$$n_\infty(\epsilon_0) = p(\epsilon_0) \tau(\epsilon_0). \quad (2)$$

If one wants to fill a trap with UCN up to a cutoff energy set by the trapping potential  $V_{\text{trap}}$ , what matters is the saturated total UCN density which is obtained from

$$n_\infty = \int_0^{V_{\text{trap}}} n_\infty(\epsilon_0) d\epsilon_0. \quad (3)$$

Many applications of UCN sources involve filling external traps with as many UCN as possible, followed by a long time for holding or manipulation, during which the density in the source can be refreshed. Therefore  $n_\infty$  is a useful parameter of the converter to be optimized<sup>1</sup>.

---

<sup>1</sup>For experiments involving external traps with poor storage properties it will be better to drain UCN frequently from a partially charged source. However, also in this case a long UCN storage time constant is an asset as it will raise the time-averaged UCN content of the converter.

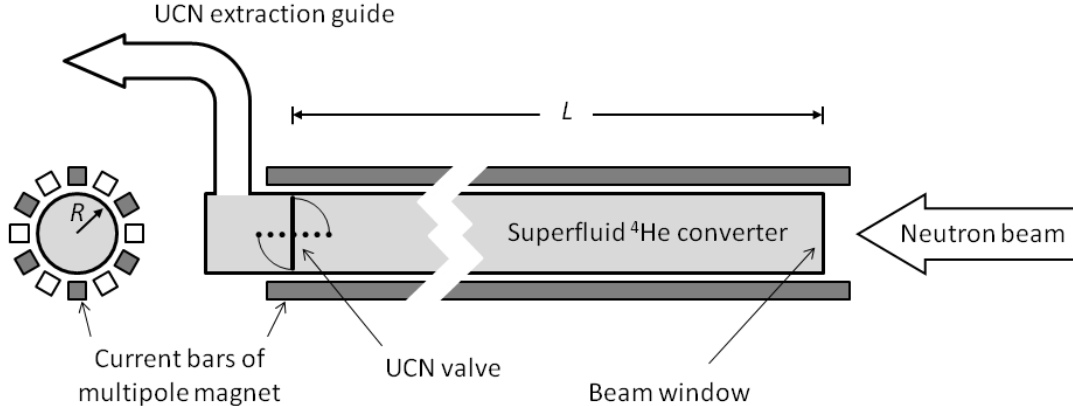


Figure 1: Schematic of the UCN accumulator comprized of a superfluid  $^4\text{He}$  converter with multipole magnet and system for UCN extraction. On the left a cut view is shown for  $n = 12$ ; filled (open) squares indicate electric current flowing into (out of) the plane. The neutron optical potentials are:  $V$  for the cylindrical inner surface over the length  $L$ ,  $\tilde{V}$  at the beam window and at the UCN valve,  $\geq \tilde{V}$  for the UCN extraction system, and  $V_{\text{He}} \approx 18.5$  neV in the superfluid.

We consider a system as schematically shown in Fig. 1. A cylindrical converter vessel with diameter  $2R$  is situated within a multipole magnet and illuminated homogeneously by a cold neutron beam passing along the  $r = 0$  axis. UCN accumulation takes place over a length  $L \gg R$  between a beam window and a UCN valve fully immersed in the helium as in the apparatus described in [69]. Shown is a butterfly valve but also different types may be envisaged, such as an iris diaphragm valve. For experiments at room temperature UCN are released into a window-less extraction system with a short vertical guide section as described in [61]<sup>2</sup>. In the section for UCN accumulation the cylindrical wall possesses a neutron optical potential  $V + iW$  [1, 4, 5], with

$$V = \frac{2\pi\hbar^2}{m_n} \sum_l N_l b_l, \quad W = \frac{\hbar}{2} \sum_l N_l v \sigma_l(v), \quad (4)$$

where  $m_n$  is the neutron mass,  $N_l$  is the atomic number density of the nuclear species  $l$  with coherent bound neutron scattering length  $b_l$ , and  $\sigma_l(v)$  is the loss cross section (sum of cross sections for neutron capture and upscattering;  $v$  is the UCN velocity in the medium and  $v\sigma_l(v)$  usually constant over the whole UCN spectrum). The beam window and the UCN valve are made of (or coated with) a material with neutron optical potential  $\tilde{V} + i\tilde{W}$ .

A radial  $n$ -polar magnetic field with modulus

$$B(r) = B_R \left(\frac{r}{R}\right)^{\frac{n}{2}-1} \quad (5)$$

can be generated as shown, using a regular arrangement of an even number of  $n$  straight current bars on the outer cylinder surface, with opposite current in adjacent bars (in practice one employs long racetrack coils). A neutron moving in such a field has a magnetic potential energy of

$$V_m(r) = \pm V_{mR} \left(\frac{r}{R}\right)^{\frac{n}{2}-1}, \quad V_{mR} = |\mu_n| B_R, \quad (6)$$

<sup>2</sup>It is also conceivable to place the UCN valve closer to (or within) the extraction guide. This would however considerably increase the surface of wall material exposed to the UCN during accumulation. Here we analyse the system as shown in fig. 1.

where the upper (lower) sign in this and all subsequent equations describes neutrons in the low (high) field seeking spin state, denoted by lfs and hfs in the sequel. Note that we assume adiabatic spin transport and thus neglect spin flip transitions. It is an experimentally established fact that the validity of the adiabatic condition can be fulfilled better than needed for our purposes, using a weak bias field in the order of a few 10 mT along the axis of the multipole magnet. For instance, an octupole trap has provided UCN storage lifetimes in the order of 800 s. Losses occurred primarily due UCN hitting a teflon piston coated with fomblin grease, which was used for axial closure of the trap [70]. A storage lifetime much closer to the neutron lifetime was attained in a 20-pole magnetic trap, in which UCN were held without any wall collisions [71].

Due to addition of magnetic fields to the neutron optical potentials, trapping of UCN can become strongly spin-dependent. The trapping potential of the converter vessel shown in Fig. 1 is given by

$$V_{\text{trap}} = \min \left( (V \pm V_{mR} - V_{\text{He}}) \Theta (V \pm V_{mR} - V_{\text{He}}), \left( \tilde{V} - V_{\text{He}} \right) \Theta \left( \tilde{V} - V_{\text{He}} \right) \right), \quad (7)$$

i.e. the minimum of the total potential (neutron optical wall potential and magnetic interaction potential, reduced by the neutron optical potential of the converter medium). The first argument describes the situation at the cylindrical wall (with potential  $V$ ), the second one at the end disks (potential  $\tilde{V} \geq V$ ). The expression employs the step function  $\Theta(x) = 1$  for  $x > 0$  and  $\Theta(x) = 0$  for  $x \leq 0$ , and

$$V_{\text{He}} \approx 18.5 \text{ neV} \quad (8)$$

is the neutron optical potential of the superfluid  $^4\text{He}$  as calculated using eq. 4 with  $N_{\text{He}} \approx 2.18 \times 10^{22} \text{ cm}^{-3}$  and  $b_{\text{He}} \approx 3.26 \times 10^{-13} \text{ cm}$ . For the lfs neutrons the lowest potential energy prevails on the line  $r = 0$ , whereas for the hfs neutrons it has its minimum close to the cylindrical wall (see Fig. 2). Note however that the hfs neutrons will only be able to leave the magnetic field if they still possess kinetic energy at  $r = 0$  and hence only for  $\epsilon_0 > V_{mR}$  according to our previous definition of  $\epsilon_0$ . Since we are not further interested in the fate of hfs neutrons unable to escape the multipolar field after opening the UCN valve, and for simplicity of the equations to follow, we define  $\epsilon_0$  in the sequel commonly for both spin states as the kinetic energy in the point of lowest magnetic field (i.e. on the line  $r = 0$ ). Equation 3 thus describes, individually for both spin states, UCN densities of useable UCN (i.e. those with  $\epsilon_0 > 0$ ), with  $V_{\text{trap}}$  as defined in eq. 7. We define the polarization of the saturated ensemble of useable UCN as

$$P_{\infty} = \frac{n_{\infty, \text{lfs}} - n_{\infty, \text{hfs}}}{n_{\infty, \text{lfs}} + n_{\infty, \text{hfs}}}. \quad (9)$$

As shown in Fig. 2 for two situations it will depend on the relative strengths of magnetic and neutron optical potentials.

### 3 UCN losses from the converter

The inverse of the time constant appearing in the loss term in eq. 1 is comprized of several contributions,

$$\tau^{-1}(\epsilon_0, T) = \tau_{\text{wall}}^{-1}(\epsilon_0) + \tau_{\text{slit}}^{-1}(\epsilon_0) + \tau_{\text{up}}^{-1}(T) + \tau_{\text{abs}}^{-1} + \tau_{\text{depol}}^{-1}(\epsilon_0) + \tau_{\beta}^{-1}, \quad (10)$$

where the argument indicates now also the dependence on the temperature  $T$  of the converter. From left to right, they describe UCN loss at collisions with the walls of the converter vessel, escape of UCN through an imperfectly closed UCN valve and through slits caused by manufacturing imperfections of the vessel assembly, upscattering by thermal excitations in the helium, absorption by  $^3\text{He}$  impurities, UCN depolarization at wall collisions, and neutron beta decay.

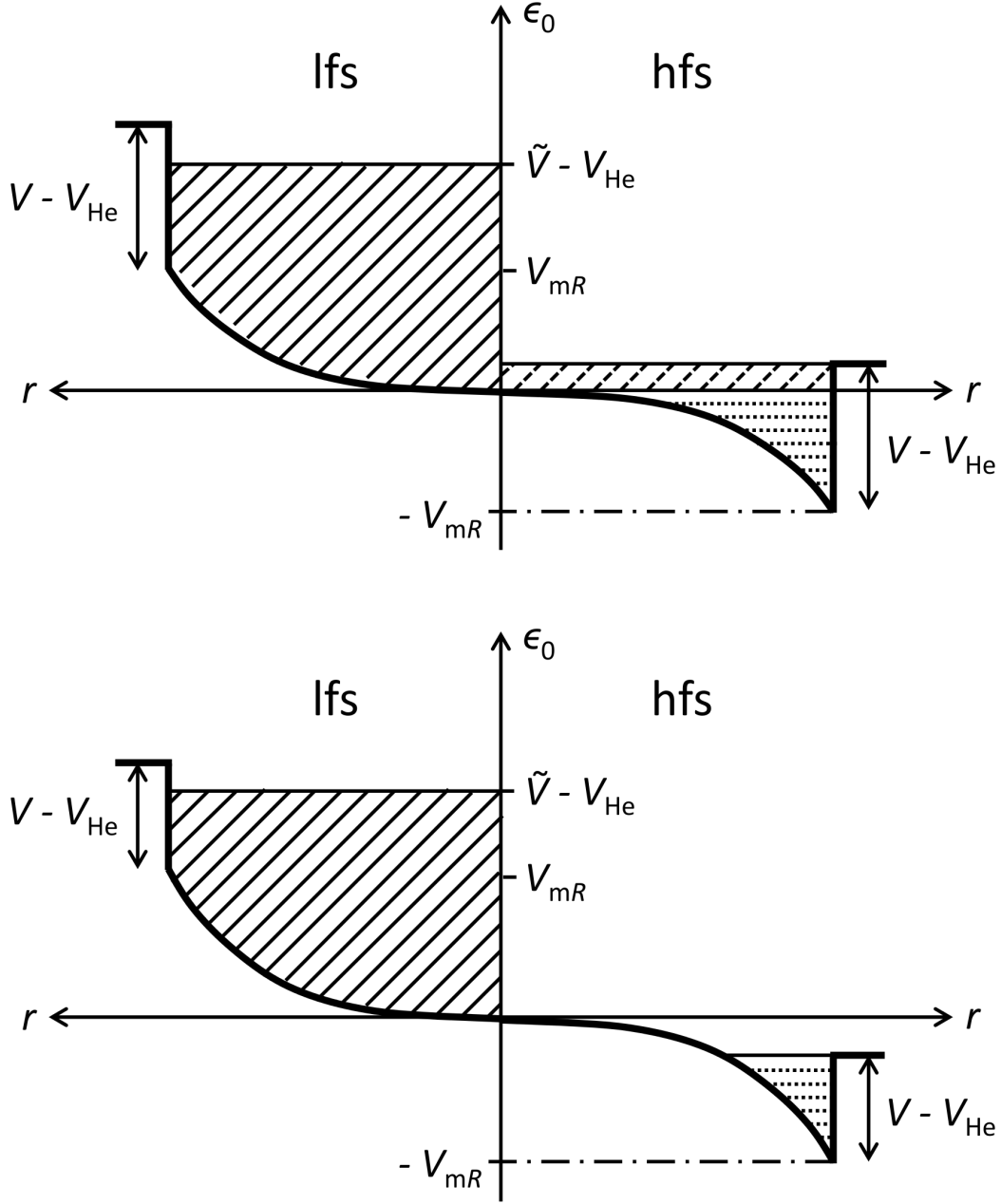


Figure 2: Schematic of the magnetic and neutron optical potentials in the closed UCN accumulator shown in Fig. 1. In the upper figure,  $V - V_{\text{He}} > V_{mR}$ . Low field seeking (lfs) UCN with total energy  $\epsilon_0 < \tilde{V} - V_{\text{He}}$  are trapped (solid line shade). High field seeking (hfs) UCN with  $0 < \epsilon_0 < V - V_{\text{He}} - V_{mR}$  are trapped, too (dashed-line shade), leading to polarization  $P_\infty < 1$  according to eq. 9. The lower figure illustrates the situation  $V - V_{\text{He}} < V_{mR}$  where hfs UCN with  $\epsilon_0 > 0$  are free to escape, hence  $P_\infty = 1$ . Only hfs UCN with  $\epsilon_0 < 0$  (horizontal dotted shade) are trapped which however will stay in the regions with strong magnetic field when opening the UCN valve.

Note that, using an unpolarized beam for neutron conversion, the rate constant  $\tau_{\text{depol}}^{-1}$  may become relevant only if trapping is at least partly magnetic. In an experimental study a depolarization probability per wall collision of  $7 \times 10^{-6}$  was measured for a bottle made of Be [72]. Hence,  $\tau_{\text{depol}}^{-1} < \tau_{\beta}^{-1}$  even for the fastest neutrons in the narrow trap geometry discussed here. Like the first two rate constants in eq. 10,  $\tau_{\text{depol}}^{-1}$  will be further suppressed due to the multipole magnet (provided that spin transport is adiabatic), and we therefore neglect it. For temperatures below 1 K [69, 73],

$$\tau_{\text{up}}^{-1}(T) \approx \frac{(T[\text{K}])^7}{100 \text{ s}}, \quad (11)$$

so that for  $T < 0.5$  K,  $\tau_{\text{up}}^{-1}$  contributes with less than 10% of  $\tau_{\beta}^{-1}$ . The rate constant  $\tau_{\text{abs}}^{-1}$  can be suppressed below any relevant level by purification of the helium from  $^3\text{He}$  using a superleak [61, 74, 75] or the heat flush technique [76]. As a result, we are left with  $\tau_{\text{wall}}^{-1}$  and  $\tau_{\text{slit}}^{-1}$  as dominating contributions, and the rate constant due to neutron decay sets an ultimate lower limit for a perfect converter.

For the losses due to wall collisions we want to apply an analytic description. If we assume the trapped UCN in mechanical equilibrium we can use formulas derived in the book [4] where the authors analyzed the effect of the earth's gravitational field on neutrons moving in a bottle. We adapt the notation to our case and replace the height parameter  $h$  by the radial coordinate  $r$  characterizing the multipolar magnetic field strength. We neglect the gravitational field, which is a good approximation for a horizontal source with less than 10 cm diameter. The kinetic neutron energy for the two spin states is then given by  $E(r) = \epsilon_0 \mp |V_{\text{m}}(r)|$ . The energy,

$$E := E(R) = \epsilon_0 \mp V_{\text{m}R}, \quad (12)$$

is positive for the extractable hfs neutrons which can always explore the whole trap. The low field seeking neutrons on the other hand may have too low energy to hit the walls. For  $E > 0$  eq. 12 defines the energy of neutron impact. Employing a formula given in ref. [4], the angular averaged probability  $\bar{\mu}(E)$  for UCN loss during a collision with the cylindrical wall of the helium filled converter vessel can be written as

$$\bar{\mu}(E) = 2f \operatorname{Re} \left( \frac{V'}{E} \arcsin \sqrt{\frac{E}{V'}} - \sqrt{\frac{V'}{E} - 1} \right) \quad \text{for } E \leq V', \quad (13)$$

valid for a neutron optical potential  $V + iW$  with small losses, i.e.  $f = W/V \ll 1$ , and writing

$$V' = V - V_{\text{He}}, \quad (14)$$

with  $V_{\text{He}}$  given in eq. 8. For convenience in later calculations we have included a projection onto the real part of the expression. It offers a handy formulation of the case where neutrons have too low energy to hit the wall, ensuring that  $\bar{\mu}(E < 0) = 0$  without need to specify the range of  $E$  in advance as positive. The function  $\bar{\mu}(E)$  rises monotonously with  $E$  from  $\bar{\mu} = 0$  for  $E = 0$  to  $\bar{\mu} = \pi f$  for  $E = V'$ . For  $E > V'$  we may set  $\bar{\mu} = 1$  since we are not interested here in calculating the dynamics of marginally trapped neutrons. For  $E = V'/2$ ,  $\bar{\mu} \approx 1.14f$ . Note that, since we consider a long trap for which  $2\pi RL \gg \pi R^2$ , we will neglect losses due to  $\widetilde{W}$  at the end disks. The magnetic multipole suppresses wall losses of lfs UCN for several reasons. First, only a fraction of them has sufficient energy to hit the lossy wall. Second, those lfs neutrons with  $\epsilon_0 > V_{\text{m}R}$  hit the wall due to magnetic deceleration with a reduced kinetic energy  $E$  (eq. 12), leading to reduced losses due to  $\bar{\mu}(\epsilon_0 - V_{\text{m}R}) < \bar{\mu}(\epsilon_0)$ . Third, the rate of wall collisions of these neutrons is reduced as well, leading to a further suppression in the expressions for  $\tau_{\text{wall}}^{-1}$  and  $\tau_{\text{slit}}^{-1}$ , which we calculate next.

$n \setminus \frac{\epsilon_0}{V_{mR}}$	$\frac{1}{10}$	$\frac{1}{5}$	$\frac{1}{2}$	1	$\frac{4}{3}$	$\frac{8}{5}$	2
4	0.005	0.021	0.133	0.533	0.696	0.758	0.813
6	0.067	0.133	0.333	0.667	0.778	0.822	0.862
8	0.159	0.252	0.465	0.739	0.824	0.859	0.89
10	0.248	0.351	0.555	0.785	0.855	0.883	0.909
12	0.325	0.429	0.619	0.818	0.876	0.9	0.922
14	0.39	0.492	0.667	0.841	0.892	0.913	0.932

Table 1: Values for  $\gamma'$  for low field seeking neutrons, as defined with the upper sign in eq. 18 for various values of  $\epsilon_0/V_{mR}$ .

In mechanical equilibrium, a group of neutrons with total energy in the range  $(\epsilon_0, \epsilon_0 + d\epsilon_0)$  will occupy the accessible phase space in the trap with uniform density. As a result of phase space transformation under the influence of a conservative potential (see section 4.3.1 in the book [4]), the real space spectral UCN densities in different positions are related by

$$n(\epsilon_0, t, r) = \text{Re} \sqrt{\frac{\epsilon_0 \mp |V_m(r)|}{\epsilon_0}} n(\epsilon_0, t, 0), \quad (15)$$

where projection onto the real part ensures  $n(\epsilon_0, t, r) = 0$  for the lfs UCN for  $r > R^*$  defined by  $\epsilon_0 = |V_m(R^*)|$ . We define an effective volume of the source for neutrons with total energy  $\epsilon_0$  as

$$\gamma(\epsilon_0) = 2\pi L \text{Re} \int_0^R \sqrt{\frac{\epsilon_0 \mp |V_m(r)|}{\epsilon_0}} r dr. \quad (16)$$

The spectral UCN density averaged over the entire volume of the converter is then given by

$$n(\epsilon_0, t) = \gamma'(\epsilon_0) n(\epsilon_0, t, 0), \quad (17)$$

and the reduced quantity,

$$\gamma'(\epsilon_0) = \frac{\gamma(\epsilon_0)}{\pi R^2 L} = 2 \text{Re} \int_0^1 \sqrt{1 \mp \frac{V_{mR}}{\epsilon_0} r^{\frac{n}{2}-1}} r dr, \quad (18)$$

was derived using eq. 6. Values for  $\gamma'$  listed in Table 1 show that, the higher the multipolarity, the less significant becomes the reduction of the density of the lfs neutrons with respect to a square well potential of same depth. The spectral current density of neutrons at any point in the vessel, per unit area and per energy interval about  $\epsilon_0$ , is given by the gas kinetic relation

$$J(\epsilon_0, t, r) = \frac{1}{4} n(\epsilon_0, t, r) v(\epsilon_0, r). \quad (19)$$

The spectral rate of UCN collisions with the cylindrical wall of the helium container is given by  $2\pi R L J(\epsilon_0, t, R)$ . The speed  $v(\epsilon_0, R)$  of the neutrons as they hit the wall is related to the speed at  $r = 0$  through

$$v(\epsilon_0, R) = \text{Re} \sqrt{\frac{\epsilon_0 \mp V_{mR}}{\epsilon_0}} v(\epsilon_0, 0). \quad (20)$$

With eq. 15 we obtain

$$J(\epsilon_0, t, R) = \frac{\epsilon_0 \mp V_{mR}}{\epsilon_0} J(\epsilon_0, t, 0) \Theta(\epsilon_0 \mp V_{mR}), \quad (21)$$



with the step function  $\Theta(x)$  as already used in eq. 7. For the loss term in eq. 1 due to collisions with the cylindrical wall we can thus write

$$\frac{n(\epsilon_0, t)}{\tau_{\text{wall}}(\epsilon_0)} = \frac{2}{R} \bar{\mu}(\epsilon_0 \mp V_{\text{m}R}) J(\epsilon_0, t, R). \quad (22)$$

Further evaluation using eq. 21, eq. 19 for  $r = 0$ , eq. 17, and inserting  $\bar{\mu}$  from eq. 13 leads us to

$$\tau_{\text{wall}}^{-1}(\epsilon_0) = \frac{v(\epsilon_0, 0)}{R\gamma'(\epsilon_0)} f \frac{V'}{\epsilon_0} \text{Re} \left( \arcsin \sqrt{\frac{\epsilon_0 \mp V_{\text{m}R}}{V'}} - \sqrt{\frac{\epsilon_0 \mp V_{\text{m}R}}{V'}} \left( 1 - \frac{\epsilon_0 \mp V_{\text{m}R}}{V'} \right) \right). \quad (23)$$

For the calculation of the corresponding expression for losses through slits it is reasonable to assume them to be situated at  $r = R$ , e.g. at the seam of the tube or at its connections to the circular windows for the cold beam. Assuming that any UCN hitting a slit will be lost and denoting the total surface of all slits by  $A$ , their contribution to the loss term in eq. 1 is given by

$$\frac{n(\epsilon_0, t)}{\tau_{\text{slit}}(\epsilon_0)} = \frac{2}{R} \frac{A}{2\pi RL} J(\epsilon_0, t, R), \quad (24)$$

neglecting the small surface of the disks at the ends. Hence,

$$\tau_{\text{slit}}^{-1}(\epsilon_0) = \frac{Av(\epsilon_0, 0)}{4\gamma(\epsilon_0)} \frac{\epsilon_0 \mp V_{\text{m}R}}{\epsilon_0} \Theta(\epsilon_0 \mp V_{\text{m}R}), \quad (25)$$

and we see that, for the lfs neutrons, the ordinary gas kinetic expression represented in the first fraction on the right side becomes reduced for  $V_{\text{m}R} > 0$  for the same reason as the wall losses discussed before.

## 4 UCN production

We first consider UCN production in absence of the magnetic multipole field. For homogeneous irradiation with the cold neutron beam guided through the converter, neglecting decrease of intensity due to reflection losses and neutron scattering in the helium, the UCN production rate density is position independent and given by

$$p_0 = \int_0^{V_{\text{trap}}} p_0(\epsilon_0) d\epsilon_0 = KV_{\text{trap}}^{3/2}. \quad (26)$$

The  $V_{\text{trap}}^{3/2}$  dependence follows for a homogeneous population of states within a sphere in momentum space with spectral UCN production rate density

$$p_0(\epsilon_0) = \frac{3}{2} K \sqrt{\epsilon_0}. \quad (27)$$

The factor  $K$  due to single phonon emission has been calculated on the basis of neutron scattering data and confirmed in several experiments [77, 62, 78, 79, 80, 81, 82], albeit with modest experimental accuracy limited by detection efficiency and other corrections. For UCN with maximum energy determined by  $V_{\text{trap}} = V - V_{\text{He}} \approx 233 \text{ neV}$  for Be or Ni with natural isotopic composition, it is given by

$$K \approx 5\text{s}^{-1}\text{cm}^{-3} \Phi_{0.89\text{nm}} [10^9 \text{cm}^{-2}\text{s}^{-1}\text{nm}^{-1}] / (233\text{neV})^{3/2}, \quad (28)$$

where  $\Phi_{0.89\text{nm}}$  is the differential unpolarized neutron flux density at a neutron wavelength of 0.89 nm. The flux unit is chosen numerically close to values available at existing facilities, e.g.

$n \setminus \frac{V_{mR}}{V_{\text{trap}}}$	1	$\frac{3}{4}$	$\frac{5}{8}$	$\frac{1}{2}$
4	0.229	0.37	0.456	0.551
6	0.4	0.517	0.585	0.659
8	0.512	0.609	0.665	0.725
10	0.589	0.672	0.72	0.77
12	0.645	0.718	0.759	0.802
14	0.688	0.752	0.788	0.827

Table 2: Values for  $\kappa$  as defined in eq. 32 for various values of  $n$  and  $V_{mR}/V_{\text{trap}}$ .

the monochromatic beam H172A at the ILL [47]. An additional, usually smaller contribution to UCN production is due to multi-phonon processes.

When adding the multipolar magnetic field, the spectral UCN production rate density becomes dependent on position and spin state,

$$p_{\text{lfs(hfs)}}(\epsilon_0, r) = \frac{3}{4}K(r) \text{Re} \sqrt{\epsilon_0 \mp |V_m(r)|}, \quad (29)$$

where the  $r$  dependence of  $K$  accounts for a spatially varying flux density of the neutron beam. The factor  $1/2$  with respect to eq. 27 holds for an unpolarized beam incident on the converter, as always assumed hereafter. For homogeneous irradiation,  $K(r) = K$ , and the spatially averaged spectral UCN production rate density for the two spin states can be expressed in terms of the normalized effective volume from eq. 18, i.e.

$$p_{\text{lfs(hfs)}}(\epsilon_0) = \frac{3}{4}K\gamma'(\epsilon_0) \sqrt{\epsilon_0}. \quad (30)$$

Without magnetic field,  $p_{0,\text{lfs}} = p_{0,\text{hfs}} = p_0/2$  with  $p_0$  given in eq. 26, whereas with field,

$$p_{\text{lfs(hfs)}} = \int_0^{V_{\text{trap}}} p_{\text{lfs(hfs)}}(\epsilon_0) d\epsilon_0 \quad (31)$$

are different due to the spin-dependent  $\gamma'(\epsilon_0)$  and  $V_{\text{trap}}$  from eq. 7. We note particularly that the ratio of total production rates for lfs UCN with the magnetic multipole switched on and switched off,

$$\kappa = \frac{p_{\text{lfs}}}{p_{0,\text{lfs}}}, \quad (32)$$

is smaller than unity due to the phase space reduction by the magnetic multipole. The values quoted in Table 2 demonstrate a positive effect of high multipolar order  $n$  on  $\kappa$  and hence on the saturated UCN density calculated in the next section. There are however practical limits. First, thermal insulation between the magnet and the much colder helium container necessitates an annular gap over which the field would drop too strongly if  $n$  is chosen too large. Second, the maximum field strength achievable with a given maximum current density in the current bars around the converter of given diameter decreases with  $n$ . For  $R = 5$  cm, and taking into account the results given in the next section,  $n \approx 12$  turns out to be a reasonable choice.

## 5 Saturated UCN density

The spatially averaged saturated spectral densities for lfs and hfs UCN follow from eq. 2 with eq. 30, i.e.

$$n_{\infty,\text{lfs(hfs)}}(\epsilon_0) = \frac{3}{4}K\gamma'(\epsilon_0) \sqrt{\epsilon_0} \tau(\epsilon_0), \quad (33)$$

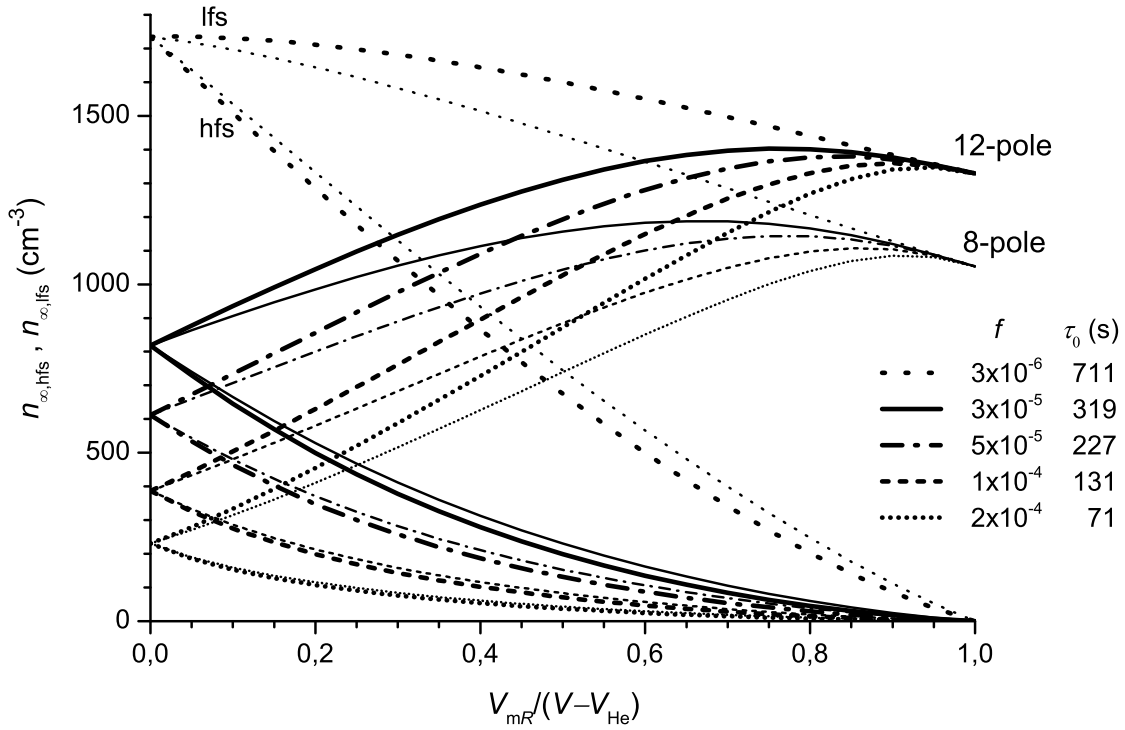


Figure 3: Saturated densities of low field and high field seeking UCN in a converter vessel with diameter 10 cm, held at 0.5 K and surrounded by a 12-pole, respectively, 8-pole magnet. Calculations employ eq. 34 for  $\tilde{V} = V = 252$  neV (e.g. for a converter vessel made entirely of Be), and for various values of  $f = W/V$ . The solid lines show results for the best value of  $f$  previously achieved for Be, while the upmost curves show the situation for unrealistically low  $f$  for illustration. Values are given for an unpolarized differential neutron flux density of  $\Phi_{0.89\text{nm}} = 10^9 \text{ cm}^{-2}\text{s}^{-1}\text{nm}^{-1}$  at  $\lambda = 0.89$  nm, as available at the monochromatic beam position H172A at the ILL. A characteristic time constant  $\tau_0$  is calculated for neutrons with velocity  $v = \frac{3}{4}v_{\text{max}}$ , including in eq. 10 the rates  $\tau_{\beta}^{-1}$ ,  $\tau_{\text{up}}^{-1}$  and the wall collisional losses calculated using eq. 23 for  $V_{mR} = 0$  and  $\epsilon_0 = \frac{9}{16}V_{\text{trap}}$ .

using the corresponding sign in eqs. 18 and in the expression for  $\tau(\epsilon_0)$ . Hence, using eq. 3 and writing out all arguments relevant for characterizing the multipolar magnetic field and the converter, the saturated total mean UCN densities in the converter are given by

$$n_{\infty, \text{lfs(hfs)}}(R, V_{mR}, n, V, f, \tilde{V}, T) = \frac{3}{4}K \int_0^{V_{\text{trap}}} \frac{\gamma'(\epsilon_0, V_{mR}, n) \sqrt{\epsilon_0}}{\tau^{-1}(\epsilon_0, R, V_{mR}, n, V, f, T)} d\epsilon_0. \quad (34)$$

The dependence on  $\tilde{V}$  is contained in the upper limit of integration, see eq. 7. From the various contributions to the rate constant  $\tau^{-1}$  (see eq. 10) we retain the terms due to wall collisions, upscattering (eq. 11) and neutron beta decay, assuming that the wall losses can entirely be described by eq. 23 and that there is no  $^3\text{He}$  in the converter and no slit in the vessel.

A first calculation of  $n_{\infty, \text{lfs}}$  and  $n_{\infty, \text{hfs}}$  was performed for a vessel featuring the neutron optical potential of Be at all walls (i.e.  $\tilde{V} = V = 252$  neV). Beryllium has become a standard material for UCN trapping, with a best reported experimental value of  $f = 3 \times 10^{-5}$  in the low temperature limit [83, 84], despite a much smaller theoretical value (the finding that this was never

reached was termed "anomalous losses" and has triggered many experimental investigations and speculations). However, it might be more realistic to consider also worse values for  $f$ , assuming that efficient cleaning procedures cannot be applied in situ (e.g. baking is excluded in presence of indium seals). Figure 3 shows results exemplary for multipole order  $n = 8$  and  $n = 12$ , as a function of the magnetic trapping potential at the cylindrical wall of the vessel, normalized to the trapping depth without magnetic field. The density of lfs UCN increases with  $n$  as expected due to the increase in trapping phase space, while that of the hfs neutrons decreases. Hence, for partial magnetic trapping of the lfs neutrons (characterized by  $V_{mR} < V - V_{\text{He}}$ , see Fig. 2), higher multipole order leads to higher UCN polarization defined in eq. 9. For instance, for a 12-pole with  $B_R = 2.5$  T, one obtains  $P_\infty = 86\%$  for  $f = 3 \times 10^{-5}$  while for a worse  $f = 2 \times 10^{-4}$  it improves to  $P_\infty = 97\%$ . As also obvious from the curves, the poorer the neutron optical UCN storage performance, the larger will be the improvement of lfs UCN density due to the multipole magnet. For the experimental cases reported in the introduction, with measured loss rate ratios as high as  $\tau^{-1}/\tau_\beta^{-1} \simeq 5.5$  [39], respectively 13 [60], a multipole magnet would indeed be very useful. Some of the curves for  $n_{\infty, \text{lfs}}$  exhibit a maximum for values  $V_{mR}/V_{\text{trap}} < 1$ . This can be understood as resulting from the competition of storage time constant  $\tau$  and the effective trap volume  $\gamma'$  entering eq. 34. For bad values of  $f$  the optimum obtains for  $V_{mR}/V_{\text{trap}}$  close to 1, while for a trap with excellent storage properties the multipole field reduces the UCN density even at low field values because the factor  $\gamma' < 1$  then dominates over a marginal gain in  $\tau$ . For illustration of this behaviour we also added a curve for an unrealistic converter vessel with hypothetical  $f = 3 \times 10^{-6}$ .

Next we consider an interesting further opportunity for buildup of a high lfs UCN density which takes advantage of the fact that the multipole magnet increases not only storage time constants but also the potential energy of the neutron at the cylindrical wall. As a result, the trapping depth of the converter vessel becomes larger if the disks providing axial confinement are made of a material with larger neutron optical potential  $\tilde{V} > V$  (remember eq. 7 and see Fig. 1). Since the surface of the disks is small, one may even employ materials which would be unsuitable for the entire vessel, for an unfavorably large  $\tilde{f} = \tilde{W}/\tilde{V}$  or because coating the tubular section with sufficient quality might be unavailable. While diamondlike carbon has already been studied in some detail [85, 86, 87, 88], further candidate materials able to extend the spectrum for UCN trapping beyond the Be cutoff have been the scope of recent investigations [89]. Particularly promising is boron nitride in the cubic phase (cBN). Its neutron optical potential of 324 neV is even larger than that of diamond (304 neV) but due to the large absorption cross section of the isotope  $^{10}\text{B}$ ,  $\tilde{f} = 1.5 \times 10^{-2}$  is also excessively large. Enrichment of the weakly absorbing  $^{11}\text{B}$  however may reduce  $\tilde{f}$  down to  $3.3 \times 10^{-5}$ , along with a further increase of  $\tilde{V}$  to a theoretical value of 351 neV. Using experiments on transmission with time-of-flight analysis and cold neutron reflectometry, the authors of ref. [89] have demonstrated a value of  $305 \pm 15$  neV for their 2  $\mu\text{m}$  thick deposit of cBN (with natural isotopic composition) on a circular silicon waver. The deviation from the ideal value is due to a cubic phase content of 90%, which was measured independently by IR spectroscopy. For highly enriched material, and assuming the same cubic phase content, one may expect a neutron optical potential of about 330 neV.

Figure 4 shows saturated UCN densities calculated for a trap with a Be-coated cylindrical wall with  $f = 3 \times 10^{-5}$  and with the axial UCN confinement provided by Be,  $^{11}\text{BN}$  (90% cubic), or cubic  $\text{C}_3\text{N}_4$ . The latter features an extraordinarily large theoretical value of  $\tilde{V} = 391$  neV. The curves for  $\tilde{V} > V$  for the lfs UCN start with a slope larger than in the case  $\tilde{V} = V$  (dash-dotted). This is due to a  $B_R$  dependent increase of the integration range,  $V_{\text{trap}}$ , in eq. 34, as long as  $V_{mR} < \tilde{V} - V$ . Kinks in the curves appear at magnetic field values corresponding to  $V_{mR} = \tilde{V} - V$  where the full trapping depth is reached. While for a high quality Be trap with  $\tilde{V} = V = 252$  neV the gain in UCN density is not too impressive (lowest two curves), for  $\tilde{V} = 330$  neV a magnetic 12-pole with  $B_R = 2.5$  T enhances the saturated low field seeker UCN

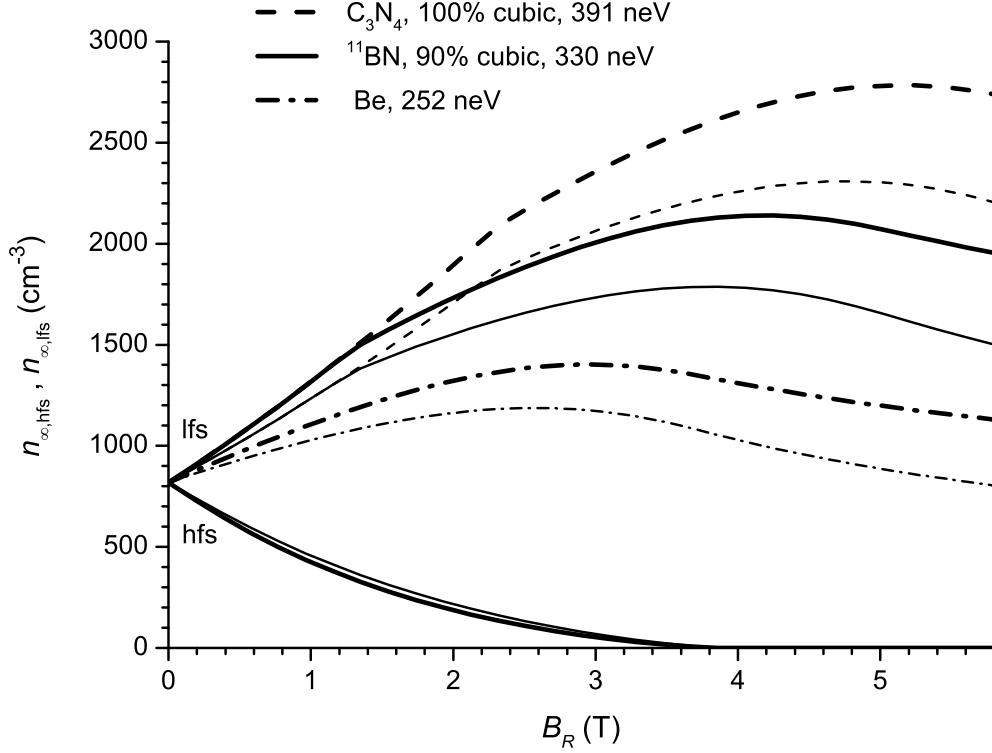


Figure 4: Saturated densities of low field and high field seeking UCN in converter vessels with diameter 10 cm,  $V = 252$  neV,  $f = 3 \times 10^{-5}$ ,  $T = 0.5$  K, and beam window and UCN valve (see Fig. 1) coated with three different materials with values of  $\tilde{V}$  as indicated in the legend. The thicker of each pair of curves is for multipolarity  $n = 12$ , the thinner for  $n = 8$ , and all values are given for  $\Phi_{0.89\text{nm}} = 10^9 \text{ cm}^{-2}\text{s}^{-1}\text{nm}^{-1}$  (unpolarized). The kinks visible for the two upper pairs of curves appear at field values corresponding to  $V_{mR} = \tilde{V} - V$ . Densities of the hfs UCN for  $\tilde{V} \geq V$  are independent on  $\tilde{V}$  but are smaller for the higher multipole order.

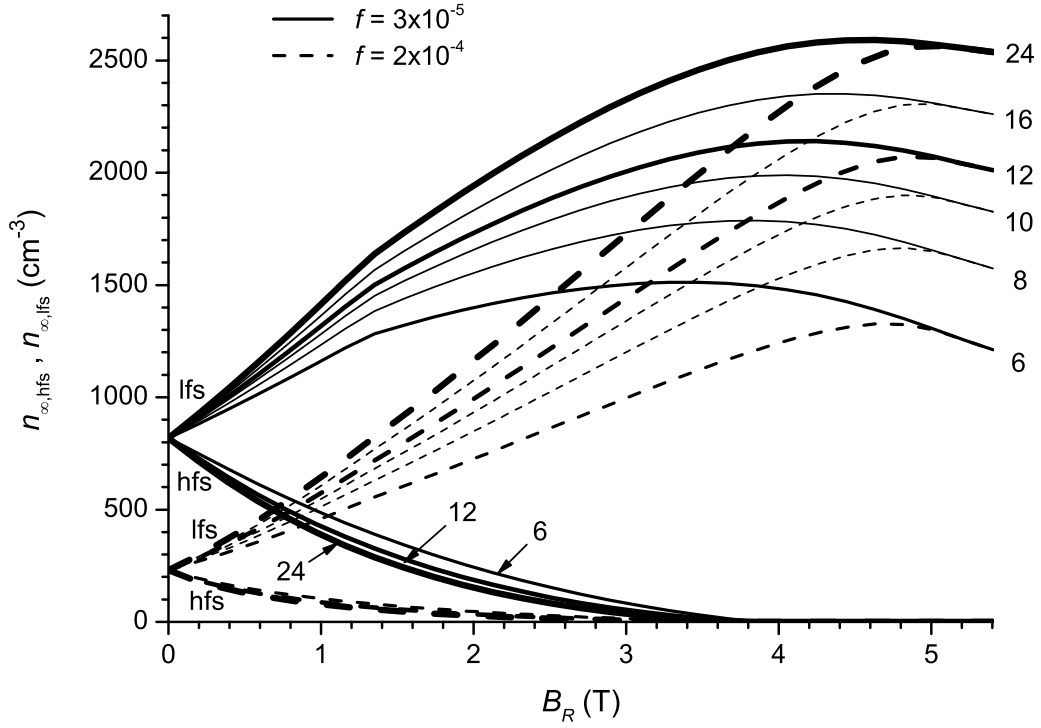


Figure 5: Saturated densities of low field and high field seeking UCN in converter vessels with diameter 10 cm,  $V = 252$  neV,  $T = 0.5$  K,  $f = 3 \times 10^{-5}$  (solid curves) or  $f = 2 \times 10^{-4}$  (dashed). Beam window and UCN valve (see Fig. 1) are coated with  $c^{11}\text{BN}$  with  $\tilde{V} = 330$  neV. The magnetic multipole order is varied between  $n = 6$  and 24. Values are given for  $\Phi_{0.89\text{nm}} = 10^9 \text{ cm}^{-2}\text{s}^{-1}\text{nm}^{-1}$  (unpolarized).

$\tilde{V}$ (neV)	$B_R$ (T)	$f$	$3 \times 10^{-5}$	$1 \times 10^{-4}$	$2 \times 10^{-4}$	$4 \times 10^{-4}$
330	2.5	$n_{\infty,\text{lfs}}$ ( $\text{cm}^{-3}$ )	1880	1430	1210	1050
		$P_{\infty}$	0.89	0.949	0.969	0.981
252	2.5	$n_{\infty,\text{lfs}}$ ( $\text{cm}^{-3}$ )	1380	1200	1080	980
		$P_{\infty}$	0.86	0.939	0.965	0.98
$\geq 252$	0	$n_{\infty,\text{lfs}}$ ( $\text{cm}^{-3}$ )	820	390	230	130
		$P_{\infty}$	0	0	0	0

Table 3: Values for the saturated density of low field seeking UCN (see eq. 34) and UCN polarization (eq. 9), for a converter vessel with  $R = 5$  cm,  $T = 0.5$  K, surrounded by a 12-pole magnet, and for several values of  $f$ . Values are given for an unpolarized differential flux density of  $\Phi_{0,89\text{nm}} = 10^9 \text{ cm}^{-2}\text{s}^{-1}\text{nm}^{-1}$ .

density  $n_{\infty,\text{lfs}}$  by a factor 2.3 from  $820 \text{ cm}^{-3}$  to  $1880 \text{ cm}^{-3}$ . Hence, if the experiment connected to the source can use the high-energy UCN it provides, the magnetic multipole is an asset even for a vessel with very good storage properties. Note that the saturated high field seeker UCN density  $n_{\infty,\text{hfs}}$  for  $\tilde{V} \geq V$  does not depend on  $\tilde{V}$ , since for them the trapping potential is given by  $V - V_{\text{m}R}$  (see upper part of Fig. 2). Hence, the larger  $\tilde{V}$ , the larger will be the polarization  $P_{\infty}$  defined in eq. 9 (see also Table 3). Note also that, as sketched in the lower part of Fig. 2, for magnetic fields providing a trapping potential stronger than the neutron optical one ( $B_R \gtrsim 3.9$  T for the situation shown in Fig. 4),  $P_{\infty} = 1$ .

Figure 5 shows the dependence of saturated UCN density on the multipole order, for traps with Be-coated cylindrical wall with  $f = 3 \times 10^{-5}$ , respectively  $f = 2 \times 10^{-4}$ , each with end windows with a potential of  $\tilde{V} = 330$  neV. Again, one notes the positive influence of higher multipole order on the number of trapped UCN and on the polarization. Table 3 quotes values for  $n_{\infty,\text{lfs}}$  and  $P_{\infty}$  for  $n = 12$  and for various values of  $f$ . One can see, for instance for  $f = 2 \times 10^{-4}$ , that the magnetic field enhances  $n_{\infty,\text{lfs}}$  by more than a factor five from  $230 \text{ cm}^{-3}$  to  $1210 \text{ cm}^{-3}$ . One also notes that the multipole field stabilizes the output of the source, by mitigating the influence of the loss coefficient of the converter wall surface. This includes possible deterioration of the wall quality with time, which will then also be much less an issue than without the field.

For application of the source for feeding a magnetic trap, e.g. for neutron lifetime experiments with typical trapping potentials in the range (50 – 120) neV (see current projects in refs. [90, 91, 63, 92, 93]), it is interesting to study the dependence of  $n_{\infty,\text{lfs}}$  on the upper bound of the trapped UCN energy spectrum. Figure 6 shows this dependence, for traps with  $n = 12$  and again with the cylindrical section made of Be with  $f = 3 \times 10^{-5}$ , respectively  $f = 2 \times 10^{-4}$ . Values are calculated using eq. 34 with the potential  $\tilde{V} - V_{\text{He}}$  set to different values starting from 60 neV and increased in steps of 20 neV. We see that, the lower  $\tilde{V}$ , the lower will be the magnetic field needed to optimize the UCN density. The reason is that lowering  $\tilde{V}$  reduces wall collisional losses due to the energy dependence of  $\bar{\mu}(E)$  defined in eq. 13 and due to wall hits occurring at a smaller rate, whereas the effective volume  $\gamma'$  decreases quickly with  $V_{\text{m}R}$  for a low-energy UCN spectrum (see Table 1). The solid curves in Fig. 6 tell us that, for the converter vessel coated with an excellent Be mirror,  $f = 3 \times 10^{-5}$ , the multipole magnet will offer some advantage only for not too low UCN cutoff energy. However, for a more realistic situation,  $f = 2 \times 10^{-4}$ , gains due to the magnet are rather significant even for low-energy UCN spectra. For example, for feeding an external trap with trapping depth 60 neV, it will improve  $n_{\infty,\text{lfs}}$  by a factor 2 at  $B_R \approx 0.8$  T. With increasing trapping depth the gain increases, e.g. to a factor 3.2 at  $B_R \approx 1.8$  T for  $V_{\text{trap}} = 120$  neV.

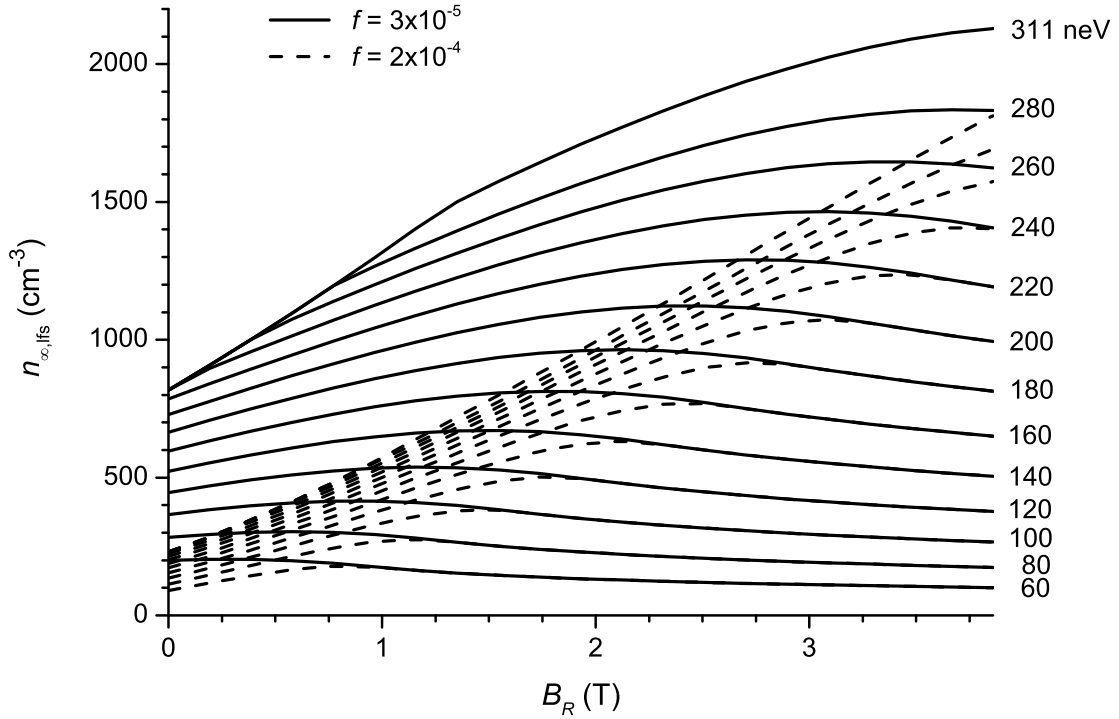


Figure 6: Saturated density of low field seeking UCN in converter vessels with diameter 10 cm,  $V = 252$  neV,  $T = 0.5$  K and surrounded by a 12-pole magnet. Solid curves are for  $f = 3 \times 10^{-5}$ , dashed ones for  $f = 2 \times 10^{-4}$ .  $\tilde{V} - V_{\text{He}}$  is varied between 60 neV and 311 neV. Values are given for  $\Phi_{0.89\text{nm}} = 10^9 \text{ cm}^{-2}\text{s}^{-1}\text{nm}^{-1}$  (unpolarized).



## 6 Conclusions

As our analysis shows, a multipole magnet can lead to a large gain in the saturated density of low field seeking UCN because the presence of the field reduces the number of neutrons hitting the material walls and reduces the energy and wall collision rate of those that do. In addition, it acts as a source-intrinsic UCN polarizer without need to polarize the incident beam and hence avoiding associated losses. A 12-pole magnet with field  $B_R = 2.5$  T on a radius of  $R = 5$  cm seems technically feasible using standard NbTi superconducting wire technology, as investigated in an independent study using a finite element code. Based on results of experimental work done by other groups, a promising candidate vessel able to provide a UCN spectrum with exceptionally high cutoff consists of a Be trap closed off by disks coated with  $c^{11}\text{BN}$ . Alternative materials are diamondlike carbon with  $V$  close to 300 neV depending on the abundance of  $\text{sp}_3$  chemical bonds, or enriched  $^{58}\text{Ni}$  with  $\bar{V} = 346$  neV and a theoretical  $f = 8.6 \times 10^{-5}$ , which however is magnetic so that UCN depolarization might be an issue that needs experimental study. We note that, in order to extract the full benefits, the incoming cold beam will need to be transported by a supermirror guide, with a top layer deposit of a good UCN reflecting material with neutron optical potential  $V$ . An experimental study of a UCN source prototype involving a converter vessel coated with such type of mirror is currently underway at the ILL, in preparation of the UCN source project SuperSUN which will include a 12-pole magnet around a 3 m long cylindrical converter vessel.

Our benchmark converter is able to provide a saturated low field seeker UCN density almost as high as an unrealistic, perfect trap with  $f = 0$  and Be cutoff, for which one calculates  $n_{\infty,\text{ifs}} = 2060 \text{ cm}^{-3}$  when exposed to a neutron beam with differential flux density  $\Phi_{0.89\text{nm}} = 10^9 \text{ cm}^{-2}\text{s}^{-1}\text{nm}^{-1}$ . For a pure Be trap equipped with the 12-pole magnet one calculates  $n_{\infty,\text{ifs}} = 1380 \text{ cm}^{-3}$  for  $f = 3 \times 10^{-5}$  as previously achieved for this material, while for  $f$  ten times worse, we still obtain  $n_{\infty,\text{ifs}} = 1110 \text{ cm}^{-3}$ . Without magnet on the other hand,  $n_{\infty,\text{ifs}}$  would get suppressed by a factor five, which impressively demonstrates the capability of the magnetic multipole reflector to mitigate the influence of a poor loss coefficient  $f$  of the converter wall surface. Obviously, also if loss of quality of the inner converter surface with time will be an issue, the magnet offers a valuable practical advantage.

Including the high field seekers into the discussion, one first notes that without magnetic field they are equally well trapped, so that in this case (and still assuming the usual situation of an unpolarized cold neutron beam for UCN production) the total UCN density in the source will be a factor two higher. However, for experiments requiring polarized UCN such as magnetic traps for precise determination of the neutron lifetime, or the neutron EDM experiment, this factor is of no use. Values for polarization of the trapped ensemble of UCN after saturation of the source were quoted in Table 3 and are typically well beyond 90% for the system discussed. As obvious from Fig. 2, low-energy UCN may stay poorly polarized whereas for the high-energy part of the spectrum the high field seekers, after magnetic acceleration to the cylindrical wall, will have kinetic energy beyond its cutoff potential and quickly get lost. Poor polarization is not a problem for experiments using magnetic traps which can be designed for quick cleaning out the wrong spin component. For experiments that would profit from a very high initial polarization one might coat the converter vessel with a low-loss material with potential  $V < V_{mR}$ , which would lead to nearly 100% UCN polarization since the high field seekers would stay untrapped. For a system with  $V > V_{mR}$  one may still, if needed, increase the polarization by delayed extraction of the UCN after having switched off the saturating neutron beam. The high field seekers will then quicker leave the trap than the low field seekers due to shorter trapping time constants. One might also cut out the lowest-energy part of the spectrum by a vertical UCN guide section with suitably chosen length.

As an important detail not affecting our conclusions we note that, in addition to the multipole

field, it will be necessary to apply a bias field in the order of some 10 mT along the converter axis to avoid depolarization in the region around  $r = 0$ , where the multipole field is zero. In addition, we can consider using axial magnetic pinch fields to increase  $V_{\text{trap}}$  and thereby the density of the UCN for an extended energy spectrum. For extraction, the field at one end needs to be ramped down, so that an iris type UCN valve might be most appropriate for this case. An extended UCN spectrum would be interesting if UCN of any velocity were beneficial, such as in UCN transmission experiments, or in combination with a phase space transformation by letting the UCN rise against the gravitational field. Note however that low-loss extraction of such a UCN spectrum will be a challenge. On the other hand, some studies might be performed in situ using static pinch fields, such as experiments on UCN upscattering in superfluid  $^4\text{He}$ , for which any increase in UCN density will be very welcome.

## References

- [1] E. Fermi, *Ricerca Scientifica* **7**, 13 (1936).
- [2] V.I. Luschikov, Yu.N. Pokotilovsky, A.V. Strelkov, F.L. Shapiro, *Sov. Phys. JETP Lett.* **9**, 23 (1969).
- [3] A. Steyerl, *Phys. Lett.* **29B**, 33 (1969).
- [4] R. Golub, D.J. Richardson, S.K. Lamoreaux, *Ultra-Cold Neutrons* (Adam Hilger, Bristol 1991).
- [5] V.K. Ignatovich, *The Physics of Ultracold Neutrons* (Oxford Science Publications, Clarendon Press, Oxford, 1990).
- [6] D. Dubbers and M.G. Schmidt, *Rev. Mod. Phys.* **83**, 1111 (2011).
- [7] M.J. Ramsey-Musolf and S. Su, *Phys. Rept.* **456**, 1 (2008).
- [8] H. Abele, *Prog. Nucl. Phys.* **60**, 1 (2008).
- [9] T. Jenke, P. Geltenbort, H. Lemmel, H. Abele, *Nature Phys.* **7**, 468 (2011).
- [10] A.P. Serebrov, E.B. Aleksandrov, N.A. Dovator et al., *Phys. Lett. B* **663**, 181 (2008).
- [11] G. Ban, K. Bodek, M. Daum et al., *Phys. Rev. Lett.* **99**, 161603 (2007).
- [12] I. Altarev, C.A. Baker, G. Ban et al., *Phys. Rev. Lett.* **103**, 081602 (2009).
- [13] T. Jenke, G. Cronenberg, J. Burgdörfer et al., *Phys. Rev. Lett.* **112**, 151105 (2014).
- [14] A.P. Serebrov, O. Zimmer, P. Geltenbort et al., *J. Exp. Theor. Phys. Lett.* **91**, 6 (2010).
- [15] O. Zimmer, *Phys. Lett. B* **685**, 38 (2010).
- [16] A.I. Frank, P. Geltenbort, M. Jentschel et al., *Phys. Atomic Nucl.* **71**, 1656 (2008).
- [17] S. Filipp, J. Klepp, Y. Hasegawa et al., *Phys. Rev. Lett.* **102**, 030404 (2009).
- [18] D.J. Richardson and S.K. Lamoreaux, *Nucl. Instr. Meth. A* **284**, 192 (1989).
- [19] D.J. Richardson, A.I. Kilvington, K. Green, S.K. Lamoreaux, *Phys. Rev. Lett.* **61**, 2030 (1988).
- [20] T. Bitter and D. Dubbers, *Phys. Rev. Lett.* **59**, 251 (1987).

- [21] S.S. Arzumanov et al., JETP Lett. **95**, 224 (2012).
- [22] A. Pichlmaier, V. Varlamov, K. Schreckenbach, P. Geltenbort, Phys. Lett. B **693**, 221 (2010).
- [23] S. Paul, Nucl. Instr. Meth. A **611**, 157 (2009).
- [24] A.P. Serebrov, V.E. Varlamov, A.G. Kharitonov et al., Phys. Rev. C **78**, 035505 (2008).
- [25] J.S. Nico, M.S. Dewey, D.M Gilliam, F.E. Wietfeldt et al., Phys. Rev. C **71**, 055502 (2005).
- [26] M.P. Mendenhall, R.W. Pattie, Y. Bagdasarova et al., Phys. Rev. C **87**, 032501 (2013).
- [27] B. Plaster, R. Rios, H.O. Back, T.J. Bowles et al., Phys. Rev. C **86**, 055501 (2012).
- [28] D. Mund et al., arXiv:1204.0013 (2012).
- [29] H. Abele, S. Baessler, D. Dubbers et al., Phys. Rev. Lett. **88**, 211801 (2002).
- [30] A. Coc, N.J. Nunes, K.A. Olive et al., Phys. Rev. D **76**, 023511 (2007).
- [31] R.E. Lopez and M.S. Turner, Phys. Rev. D **59**, 103502 (1999).
- [32] G. Mention, M. Fecher, Th. Lasserre et al., Phys. Rev. D **83**, 073006 (2011).
- [33] E.M. Purcell, and N.F. Ramsey, Phys. Rev. **78**, 807 (1950).
- [34] M. Pospelov and A. Ritz, Annals Phys. **318**, 119 (2005).
- [35] C.A. Baker et al., Phys. Rev. Lett **97**, 131801 (2006).
- [36] A.P. Serebrov, E.A. Kolomenskiy, A.N. Pirozhkov et al., Pis'ma v ZhETF **99**, 7 (2014).
- [37] I. Altarev et al., Il Nuovo Cimento **35 C**, 122 (2012).
- [38] Y. Masuda, K. Asahi, K. Hatanaka et al., Phys. Lett. A **376**, 1347 (2012).
- [39] M.G.D. van der Grinten, Nucl. Instr. Meth. A **611**, 129 (2009).
- [40] I. Altarev, G. Ban, G. Bison, K. Bodek et al., Nucl. Instr. Meth. A **611**, 133 (2009).
- [41] A.P. Serebrov et al., Nucl. Instr. Meth. A **611**, 263 (2009).
- [42] S.K. Lamoreaux and R. Golub, J. Phys. G: Nucl. Part. Phys. **36**, 104002 (2009).
- [43] The EDM@SNS neutron EDM experiment, <http://p25ext.lanl.gov/edm/edm.html>.
- [44] R. Golub and S.K. Lamoreaux, Physics Reports **237**, 1 (1994).
- [45] J. Karch, Yu. Sobolev, M. Beck et al., Eur. Phys. J. A **50**, 78 (2014).
- [46] B. Lauss, Phys. Procedia **51**, 98 (2014).
- [47] F.M. Piegsa, M. Fertl, S.N. Ivanov, K.K.H. Leung, M. Kreuz, P. Schmidt-Wellenburg, T. Soldner, O. Zimmer, Phys. Rev. C **90**, 015501 (2014).
- [48] T. Lauer, T. Zechlau, Eur. Phys. J. A **49**, 104 (2013).
- [49] A. Saunders, M. Makela, Y. Bagdasarova et al., Rev. Sci. Instrum. **84**, 013304 (2013).

- [50] Y. Masuda, K. Hatanaka, S.-C. Jeong et al., Phys. Rev. Lett. **108**, 134801 (2012).
- [51] A.P. Serebrov, V.A. Mityuklaev, A.A. Zakharov et al., Nucl. Instr. Meth. A **611**, 276 (2009).
- [52] E.I. Korobkina, B.W. Wehring, A.I. Hawari, A.R. Young et al., Nucl. Instr. Meth. A **579**, 530 (2007).
- [53] A. Frei, Y. Sobolev, I. Altarev et al., Eur. Phys. J. A **34**, 119 (2007).
- [54] U. Trinks, F. J. Hartmann, S. Paul, and W. Schott, Nucl. Instr. Meth. A **440**, 666 (2000).
- [55] R. Golub and J.M. Pendlebury, Phys. Lett. **53A**, 133 (1975).
- [56] A. Serebrov et al., J. Exp. Theoret. Phys. Lett. **59**, 11 (1994).
- [57] R. Golub, K. Böni, Z. Phys. B **51**, 95 (1983).
- [58] I. Altarev et al., Phys. Lett. A **80**, 413 (1980).
- [59] A.I. Kilvington, R. Golub, W. Mampe, P. Ageron, Phys. Lett. A **125**, 416 (1987).
- [60] O. Zimmer, F.M. Piegsa, S.N. Ivanov, Phys. Rev. Lett. **107**, 134801 (2011).
- [61] O. Zimmer, P. Schmidt-Wellenburg, M. Fertl et al., Eur. Phys. J. C **67**, 589 (2010).
- [62] O. Zimmer, K. Baumann, M. Fertl et al., Phys. Rev. Lett. **99**, 104801 (2007).
- [63] K. Leung, S. Ivanov, F. Martin et al., Proceedings of the workshop “Next Generation Experiments to Measure the Neutron Lifetime”, Santa Fe, New Mexico, 9 – 10 November 2012, page 145. World Scientific (2014).
- [64] K.K.H. Leung, O. Zimmer, Nucl. Instr. Meth. A **611**, 181 (2009).
- [65] O. Zimmer, J. Phys. G: Nucl. Part. Phys. **26**, 67 (2000).
- [66] P.R. Huffman, C.R. Brome, J.S. Butterworth et al., Nature **403**, 62 (2000).
- [67] H.S. Sommers, J.G. Dash, L. Goldstein, Phys. Rev. **97**, 855 (1955).
- [68] S.N. Dzhosyuk et al. J. Res. NIST **110**, 339 (2005).
- [69] R. Golub, C. Jewell, P. Ageron, W. Mampe, B. Heckel, I. Kilvington, Z. Phys. B **51**, 187 (1983).
- [70] K.K.H. Leung, Ph.D. thesis, TU Munich, unpublished (2013).
- [71] V.F. Ezhov, A.Z. Andreev, A.A. Glushkov et al., J. Res. NIST **110**, 345 (2005).
- [72] A. Serebrov et al., Nucl. Instr. Meth A **440**, 717 (2000).
- [73] R. Golub, Phys. Lett. **72A**, 387 (1979).
- [74] H. Yoshiki, H. Nakai, E. Gutsmedl, Cryogenics **45**, 399 (2005).
- [75] H. Yoshiki, K. Sakai, T. Kawai, S. Goto'o, Cryogenics **34**, 277 (1994).
- [76] P. McClintock, Cryogenics **18**, 201 (1978).
- [77] P. Schmidt-Wellenburg, K.H. Andersen, O. Zimmer, Nucl. Instr. Meth. A **611**, 259 (2009).

- [78] C.A. Baker, S.N. Balashov, J. Butterworth et al., Phys. Lett. A **308**, 67 (2003).
- [79] E. Korobkina, R. Golub, B.W. Wehring, A.R. Young, Phys. Lett. A **301**, 462 (2002).
- [80] Y. Masuda, T. Kitagaki, K. Hatanaka et al., Phys. Rev. Lett. **89** (2002) 284801-1.
- [81] P. Ageron, W. Mampe, R. Golub, J.M. Pendlebury, Phys. Lett. **66A**, 469 (1978).
- [82] R. Golub, J. Pendlebury, Phys. Lett. A **82**, 337 (1977).
- [83] T. Brys, M. Daum, P. Fierlinger et al., Nucl. Instr. Meth. A **551**, 429 (2005).
- [84] V. Alfimenkov et al., JETP Lett. **55**, 84 (1992).
- [85] F. Atchison, B. Blau, M. Daum et al., Nucl. Instr. Meth. B **260**, 647 (2007).
- [86] F. Atchison, B. Blau, M. Daum et al., Phys. Rev. C **74**, 055501 (2006).
- [87] F. Atchison, B. Blau, M. Daum et al., Phys. Lett. B **642**, 24 (2006).
- [88] M.G.D. van der Grinten, J.M. Pendlebury, D. Shiers et al., Nucl. Instr. Meth. A **423**, 421 (1999).
- [89] Yu. Sobolev, Th. Lauer, Yu. Borisov et al., Nucl. Instr. Meth. A **614**, 461 (2010).
- [90] V.F. Ezhov, A.Z. Andreev, G. Ban et al., arXiv:1412.7434 (2014).
- [91] D.J. Salvat, E.R. Adamek, D. Barlow et al., Phys. Rev. C **89**, 052501 (2014).
- [92] V.F. Ezhov, A.Z. Andreev, G. Ban et al., Nucl. Instr. Meth. A **611**, 167 (2009).
- [93] R. Picker, I. Altarev, J. Bröcker et al., J. Res. NIST **110**, 357 (2005).